PLOS ONE

RESEARCH ARTICLE

Impact of different biologically-adapted radiotherapy strategies on tumor control evaluated with a tumor response model

Araceli Gago-Arias[1]*, Beatriz Sánchez-Nieto[1], Ignacio Espinoza[1], Christian P. Karger[2], Juan Pardo-Montero[3,4]

1 Instituto de Física, Pontificia Universidad Católica de Chile, Santiago, Chile, **2** National Center for Radiation Research in Oncology (NCRO), Heidelberg Institute for Radiation Oncology (HIRO), Heidelberg, Germany, **3** Grupo de Imaxe Molecular, Instituto de Investigación Sanitaria (IDIS), Santiago de Compostela, Spain, **4** Servizo de Radiofísica e Protección Radiolóxica, Complexo Hospitalario Universitario de Santiago de Compostela, Santiago de Compostela, Spain

* magagoa@uc.cl

Citation: Gago-Arias A, Sánchez-Nieto B, Espinoza I, Karger CP, Pardo-Montero J (2018) Impact of different biologically-adapted radiotherapy strategies on tumor control evaluated with a tumor response model. PLoS ONE 13(4): e0196310. https://doi.org/10.1371/journal.pone.0196310

Editor: Qinghui Zhang, North Shore Long Island Jewish Health System, UNITED STATES

Received: December 4, 2017

Accepted: April 10, 2018

Published: April 26, 2018

Data Availability Statement: The relevant data underlying the findings of this study may be found at the Harvard Dataverse Network (https://dataverse.harvard.edu/) using the following citation: Gago-Arias, María Araceli; Sánchez-Nieto, Beatriz; Espinoza, Ignacio; Karger, Christian P.; Pardo-Montero, Juan, 2018, "Computational tumor models and oxygenation histograms used in the work: Impact of different biologically-adapted radiotherapy strategies on tumor control evaluated with a tumor response model"; DOI: 10.7910/DVN/JKMHMR. All other data may be found

Abstract

Motivated by the capabilities of modern radiotherapy techniques and by the recent developments of functional imaging techniques, dose painting by numbers (DPBN) was proposed to treat tumors with heterogeneous biological characteristics. This work studies different DPBN optimization techniques for virtual head and neck tumors assessing tumor response in terms of cell survival and tumor control probability with a previously published tumor response model (TRM). Uniform doses of 2 Gy are redistributed according to the microscopic oxygen distribution and the density distribution of tumor cells in four virtual tumors with different biological characteristics. In addition, two different optimization objective functions are investigated, which: i) minimize tumor cell survival (OF_{surv}) or; ii) maximize the homogeneity of the density of surviving tumor cells (OF_{std}). Several adaptive schemes, ranging from single to daily dose optimization, are studied and the treatment response is compared to that of the uniform dose. The results show that the benefit of DPBN treatments depends on the tumor reoxygenation capability, which strongly differed among the set of virtual tumors investigated. The difference between daily (fraction by fraction) and three weekly optimizations (at the beginning of weeks 1, 3 and 4) was found to be small, and higher benefit was observed for the treatments optimized using OF_{surv}. This in silico study corroborates the hypothesis that DPBN may be beneficial for treatments of tumors which show reoxygenation during treatment, and that a few optimizations may be sufficient to achieve this therapeutic benefit.

Introduction

During the last years, several studies have provided clinical evidence for the non-uniform response of tumors to radiation, mainly caused by tumor-specific heterogeneity factors such as varying oxygen supply and tumor cell proliferation and density [1]. Among these, tumor

within the paper and the Supporting Information files.

Funding: A.G-A., J.P-M and I.E. acknowledge the support of FONDECYT 2015 Postdoctoral 3150333 and FONDECYT 2017 Iniciacion 11170575, Instituto de Salud Carlos III (Miguel Servet research grant CP12/03162 and CPII17/00028), and FONDECYT 2015 Iniciacion 111505601, respectively. The funders had no role in study design, data collection and analysis, decision to publish, or preparation of the manuscript.

Competing interests: The authors have declared that no competing interests exist.

oxygenation is important because of the increased radioresistance of hypoxic cells, which can seriously affect radiotherapy treatment outcome [2–4]. In these cases, dose escalation would be required to maintain the same level of tumor control probability as compared to well-oxygenated tumors. This may, however, produce unacceptable levels of normal tissue toxicity [5, 6]. A similar situation may occur in tumors presenting a non-uniform tumor cell density distribution. As an alternative to this homogeneous dose escalation, the delivery of non-uniform dose distributions was proposed long ago to increase the efficiency of radiotherapy [7–9]. Nowadays this approach is becoming more realistic due to the capabilities of modern delivery techniques, such as IMRT. The effect associated to the delivery of non-uniform dose distributions has been evaluated both in terms of TCP and BED [10, 11]. Moreover, functional imaging techniques providing spatial-temporal information associated to biological tumor properties can provide input data for biological optimization strategies [12–14].

Despite the experimental difficulties, several studies have shown the technical feasibility to prescribe and deliver inhomogeneous dose distributions based on functional imaging (see for example the review on dose painting by Shi *et al.* [15]). Among others, dose painting by contours (DPBC) and dose painting by numbers (DPBN) are terms that are most commonly used to refer to these techniques. The DPBC technique identifies one or several regions of the planned target volume with a higher probability of local recurrence. These subvolumes are then defined as subtargets to be treated with an additional uniformly distributed dose boost [16, 17]. DPBN on the other hand, involves a voxel-based dose prescription that is calculated based on the biological information provided by functional imaging [18, 19]. Two different DPBN-strategies have been proposed: i) delivering additional dose to the less radiosensitive cells [20–22] or; ii) redistributing the dose while keeping the integral dose to the target volume constant [23, 24].

For the implementation of either DPBC and DPBN, several methodologies have been proposed to guide dose prescriptions based on functional imaging, considering: i) tumor metabolism [21, 25–29], ii) oxygenation status [16, 30–32], and iii) proliferation of tumor cells [33, 34]. Usually, they parameterize tumor control probability (TCP) or design a dose prescription function based on tracer uptakes [22, 29, 35–38].

Comparing results from the works that have addressed the clinical implementation of dose painting is however a very difficult task. Many works involved dose escalation to different dose levels, applying different adaptive schemes, and aiming at different endpoints: locoregional tumor control improvement [27, 39, 40], maximun tolerated dose [25, 41], normal tissue toxicity reduction preserving tumor control [28, 42–44], palliative response [45], etc. For this reason, and in spite of the intense research dedicated to dose painting during the last years, procedures are far from being standardized. Under such scenario, radiobiological modeling is a powerful tool that can help to study different aspects of dose painting like adaptive scheme, tumor microenvironment changes, dose prescription algorithms, etc.

In this modeling study we investigate different DPBN strategies targeting hypoxic tumors. To simulate tumor response to uniform and non-uniform dose distributions we use a previously published computational model that considers several biological processes [46]. The main objective of the study is to determine the treatment gain that could be achieved with different number of treatment adaptations (optimization). As the clinical implementation of dose painting treatments involving a large number of optimizations is non realistic nowadays due to the high logistic effort (both in terms of human resources and functional imaging tests) finding a realistic compromise between treatment gain and number of biological optimizations is mandatory.

Other relevant aspect is the method used for dose distribution optimization. In general, the spatial dose distribution in the target is a result of an optimization problem governed by an

objective function (OF). Two of the most frequently applied radiobiological optimization strategies are: i) to minimize the overall tumor cell survival (in this work referred as OF_{surv}) [9, 20, 24] and; ii) to search for the dose distribution leading to a uniform tumor cell density (OF_{std}). The latter approach assumes that a dose distribution designed to reduce biological heterogeneity within the tumor maximizes the TCP [23, 37, 47]. Although both optimization strategies would lead to a TCP higher than that of a uniform dose, the gain in treatment outcome for the different OF has not been investigated under a common methodology.

Materials and methods

Dose painting optimization methods generally involve models of cell survival, which are based on the linear quadratic (LQ) model [48]. This model accounts for the oxygen effect through oxygen enhancement ratios (OER), which are modulating factors of the fully oxic radiosensitivity parameters α and β. Using the expression of Wouters and Brown for the OERs [49], the expression for the cell survival fraction (SF) can be written as follows:

$$SF = exp[-\alpha_h OER_\alpha(p)d - \beta_h(OER_\beta(p)d)^2] \quad (1)$$

where d is the fractional dose, p is the oxygen partial tension (pO_2), α_h and β_h are the radiosensitivity parameters under hypoxic conditions and OER_α and OER_β are the oxygen enhancement ratios for α and β, respectively:

$$OER_{\alpha(\beta)} = \frac{k + p \cdot OER_{\alpha_m(\beta_m)}}{p + k} \quad (2)$$

Here, OER_{α_m} and OER_{β_m} are the maximum values of OER_α and OER_β under aerobic conditions and k is the parameter determining the slope of the curve, *i.e.* the change of OER with p. In Eq (1), α_h and β_h are equal to α/OER_{α_m} and $\beta/(OER_{\beta_m})^2$ respectively.

Regarding the oxygen tension in the tumor, the microscopic oxygen distribution rather than the average pO_2 value in a voxel should be used to calculate the oxygen-dependent tumor response [24]. The reason for this is that pO_2 values may vary on a scale much smaller than the typical voxel size and the tumor response will be governed by the most hypoxic and thus most radioresistant cells. In this work, oxygen distributions are generated by a previously published Tumor Oxygenation Model (TOM) [50] depending on the vascular fraction (vf), which is defined as tumor vascular volume fraction in the voxel, and the oxygen consumption rate. To allow efficient calculations, oxygen distributions, condensed into 16 bin pO_2-histograms, are assigned to each tumor voxel (see below).

For a virtual tumor consisting of N voxels with j levels of pO_2 each, the cell survival C_{surv} is quantified as,

$$C_{surv} = \sum_{i=1}^{N}\sum_{j=1}^{16} c_{i,j} \cdot exp[-\alpha_h OER_\alpha(p_k)d_i - \beta_h(OER_\beta(p_j)d_i)^2] \quad (3)$$

where $c_{i,j}$ is the number of tumor cells in voxel i with an oxygen pressure p_j corresponding to the *j-th* bin of the pO_2-histogram assigned to the voxel, and d_i is the dose delivered to the voxel i.

Optimization problem

Considering the cell survival presented in Eq (3), two dose redistribution optimization approaches were implemented using two different objective functions (OFs). Both are subject to the following dose constraints:

1. The average (integral) dose delivered to the virtual tumor is kept constant and equal to 2 Gy per fraction. The choice of dose redistribution, rather than dose escalation, allows comparing the results with that of standard fractionated treatments. Considering a boost would produce a higher effectiveness, not only because of the dose distribution modulation but also because of the increased energy deposition, *i.e.* integral dose to the tumor [23].
2. Dose modulation within the tumor: maximum and minimum doses ($d_{\max}$ and $d_{\min}$) are limited to differ by ±25% from the prescribed dose (2 Gy).

The objective functions investigated involved the following aproaches:

1. Minimizing the number of surviving cells (OF_{surv}):
The dose distributions minimizing the cell survival were determined according to,

$$d_i = \underset{d_{\min} \le d_i \le d_{\max}}{\operatorname{argmin}} C_{\text{surv}}, \quad \text{subject to} \quad d = \frac{1}{N}\sum_{i=1}^{N} d_i = 2Gy \tag{4}$$

2. Minimizing heterogeneity of surviving cells (OF_{std}):
The dose distributions leading to the highest spatial uniformity of cell survival were calculated by minimizing the standard deviation (*std*) of the number of surviving tumor cells within the tumor as,

$$d_i = \underset{d_{\min} \le d_i \le d_{\max}}{\operatorname{argmin}} std(C_{\text{surv}}), \quad \text{subject to} \quad d = \frac{1}{N}\sum_{i=1}^{N} d_i = 2Gy \tag{5}$$

The non-linear constrained optimization problems defined by Eqs (4) and (5) were solved using the FILTER Sequential nonlinearly constrained optimization algorithm available on the NEOS server [51, 52].

Tumor model (TOM and TMR)

In order to test the dose painting optimization strategies described above, a virtual head and neck (H&N) tumor was generated using the previously published Tumor Oxygenation Model (TOM) [50] and the Tumor Response Model (TRM) [46]. These simulation programs were developed to describe the spatial-temporal development of a given tumor, based on its biological parameters, but it may also be used to generate a virtual tumor with specified biological properties. A brief description of TOM and TRM is given in the following sections.

TOM. In this tool, microscopic pO_2 distributions are calculated in a reference tumor volume (voxel) by solving a reaction-diffusion equation [50]. This voxel is assumed to contain parallely aligned and randomly distributed linear vessels as sources of oxygen and oxygen-consuming cells outside the vessels. pO_2 distributions are calculated considering the vascular fraction, the intravascular pO_2 and the oxygen consumption rate, which depends on the fraction of dead (*i.e.*, non-consuming) cells. Oxygen distributions, summarized in pO_2-histograms, are

pre-calculated for a set of vascular and dead cells fractions and are stored for further use by the TRM.

TRM. This voxel-based multiscale model simulates the growth and radiation response of hypoxic tumors [46]. It considers viable and dead tumor cells, capillary and normal cells, as well as the most relevant biological processes such as: i) proliferation of tumor cells; ii) hypoxia-induced angiogenesis; iii) spatial exchange of cells between neighbouring voxels leading to tumor growth; iv) oxygen-dependent radiation response according to Eq (1); v) resorption of dead cells and; vi) spatial exchange of cells between neighbouring voxels leading to tumor shrinkage. By iterating through these steps, the model describes the spatial-temporal behavior of the tumor, including cell density changes, development of hypoxic cores or tumor reoxygenation arising from changes in the vascular fraction as well as from changes in the oxygen consumption. Oxygenation within each voxel is described by the oxygen histograms calculated by TOM.

Virtual tumors. Starting from a single cell, the TRM was used to grow a spherical virtual tumor of approximately 2 cm in diameter using parameters specific for a H&N-tumor. During this growth, the tumor develops a central hypoxic core of 1 cm diameter, corresponding to the gross tumor, and a 0.5 cm rim, with an increased oxygenation, representing the microscopic extension of the primary tumor. The tumor consists of 3888 cubic voxels (side length 1.124 mm) with an average cell density of $\mu = 10^6$ cells/mm^3 [53]. The tumor cell density, ρ, decreases at the tumor border such that ρ ranges from 1 to approximately 5×10^5 cells/mm^3 (see Fig 1). The resting cells in the tumor voxels are capillary cells, according to the vf, and normal cells. This virtual tumor will be referred to as tumor 1 (T1).

To study the impact of the tumor heterogeneity (distribution of ρ and vf) on the outcome of DPBN treatments, results for the tumor T1 were compared with those achieved for other three

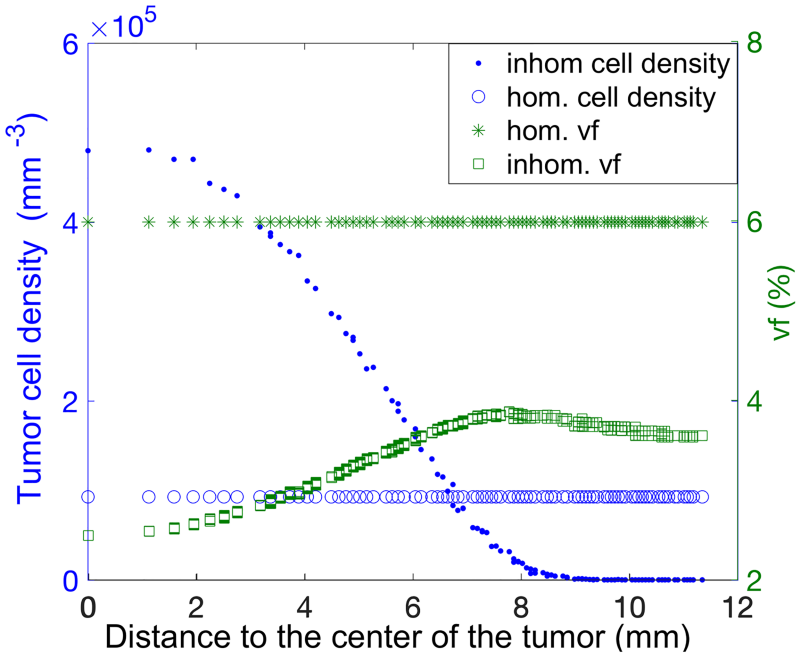

Fig 1. Radial distribution of vascular fraction and tumor cell density in the investigated virtual tumors prior to irradiation. Left axis: homogeneous (o) and inhomogeneous (.) tumor cell density distributions, ρ. Right axis: homogeneous (*) and inhomogeneous (□) vascular fraction distributions, vf. Each tumor consist of a combination of one vf and ρ profiles (see text for details).

https://doi.org/10.1371/journal.pone.0196310.g001

additional virtual tumors, referred to as T2, T3 and T4. These tumors differed either in the distribution of ρ or vf, or in the distribution of both (see Fig 1). As a result, the following tumors were investigated: T1) non-uniform distribution of ρ and vf; T2) uniform distribution of ρ and vf; T3) uniform distritubion of ρ and non-uniform distribution of vf and T4) non-uniform distribution of ρ and uniform distribution of vf.

All tumors were defined to have the same number of tumor cells. The value of vf for the uniform distribution was selected to be 6%, which is a representative value for well oxygenated tumors [54, 55]. With this vf, the oxygen effect on the optimization process is expected to be negligible. The value of ρ, used for the uniform distribution in T2 and T3 was calculated from the total number of tumor cells in T1. The biological parameters values used for the simulation of the radiation response with the TRM were the same for all tumors.

Biological parameters in the TRM. For the simulation of tumor response, parameter values representative for H&N tumors were taken from the literature (Table 1). For this, a tumor cell doubling time (t_p) of 1200 h was used at the beginning of the treatment. This slow tumor proliferation is in accordance with the Gompertzian growth of macroscopic tumors [56]. After two weeks of treatment, t_p was changed to 120 h to simulate radiation-induced accelerated repopulation [57]. The capillary cell doubling time (t_a) was set to 612 hours to simulate the slow angiogenesis process [58, 59]. The rate of dead cells resorption, characterized by the half time t_r, was considered to be equal to 168 h [60]. The radiosensitivity parameters of the LQ model were selected to be $\alpha = 0.35\ Gy^{-1}$ and $\beta = 0.035\ Gy^{-2}$, respectively [61, 62]. Additionally, a σ_α equal to $0.05\ Gy^{-1}$ was used to consider interpatient radiosensitivity variations [63, 64]. Finally, the parameter values associated to the OERs (Eq 2) were selected [49].

Considering Eqs (3)–(5) and the employed tumor model, the dose optimization was carried out considering not only the oxygen-related variation of cell radiosensitivity in the tumor, but also the distribution of tumor cells density.

Simulation studies

For each of the described virtual tumors (T1-T4), treatment response was calculated using a uniform dose distribution of 2 Gy per fraction as well as inhomogeneous dose distributions optimized using either OF_{surv} or OF_{std} (keeping the average dose equal to 2 Gy). A conventional fractionation scheme consisting of one daily fraction with two-day breaks on weekends, starting on a Monday, was simulated. These simulations were used to analyze the effect of the different objective functions in combination with different tumor characteristics.

Table 1. Biological parameters used for the simulations.

Parameters	Symbol	Value
Average cell density	μ	10^6 cells/mm^3 [53]
Tumor cell proliferation doubling time	t_p	120 and 1200 hours [56, 57]
Angiogenesis proliferation doubling time	t_a	612 hours [58, 59]
Half time of dead cell resorption	t_r	168 hours [60]
Radiosensitivity LQ-model parameters	α	$0.35\ Gy^{-1}$ [61, 62]
	β	$0.035\ Gy^{-2}$ [61, 62]
Normal std of the α parameter	σ_α	$0.05\ Gy^{-1}$ [63, 64]
Maximum value of the OER for α	OER_{α_m}	2.5 [49]
Maximum value of the OER for β	OER_{β_m}	3 [49]
OER slope parameter	k	3.28 mmHg [49]

https://doi.org/10.1371/journal.pone.0196310.t001

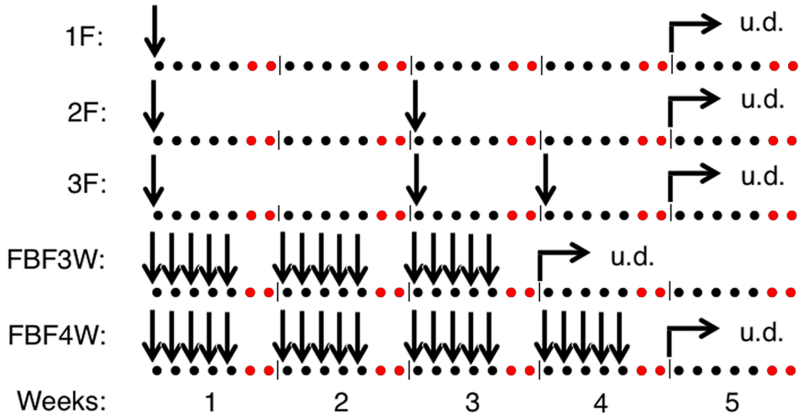

Fig 2. Time points of dose optimization within the investigated treatment schedules. Vertical arrows indicate the days (represented with dots) when dose optimization was performed. The optimized distributions are applied in all the treatment fractions from the day of optimization until a new optimization is performed. Note: No irradiations were performed at weekend (dots in red) and after 3 weeks (FBF3W) or 4 weeks (all other schedules), fractions were delivered with uniform dose (u.d. = 2Gy). The response of each virtual tumor was simulated for a uniform dose distribution as well as for the five adaptive schemes (1F, 2F, 3F, FBF3W and FBF4W) optimizing the dose distribution either with OF_{surv} and OF_{std}.

https://doi.org/10.1371/journal.pone.0196310.g002

In general, the dose distribution resulting from the optimization will depend on the biological status of the tumor, which will change during the course of irradiation. In terms of biologically adapted radiotherapy, these changes could be taken into account by daily optimization. For clinical implementation, however, this would require a daily assessment of the biological status of the tumor, *e.g.* by imaging. As this may not be feasible and since the changes in the tumor may not be so fast, a more practical approach would be to optimize the dose distribution only at certain time points of the treatment schedule. Although the best time for replanning is still a matter of debate for the clinical implementation of dose painting, there is some consensus towards doing it 1-3 weeks after treatment start [19]. We therefore simulated different adaptive schemes (see Fig 2): 1F) One fraction optimization: the dose distribution is optimized only once, at the beginning of the treatment; 2F) Two fractions optimization: the optimization is done at the beginning of the treatment and after 2 weeks of treatment; 3F) Three fractions optimization: the optimization is done at the beginning of the treatment, after 2 weeks of treatment and after 3 weeks of treatment; FBF3W) Fraction by fraction optimization: the optimization is done for every single fraction within the first 3 weeks and FBF4W) Fraction by fraction optimization: the optimization is done for every single fraction within the first 4 weeks. Uniform 2 Gy dose distributions were delivered after the 4th week of treatment in all cases with the exception of the FBF3W scheme, that continued treatment with uniform distributions already after the 3rd week.

Treatment outcome evaluation and statistical analysis. The response of the tumors was quantified in terms of cell survival and TCP curves. For the TCP calculations, tumor response was simulated at different dose levels for a population of 30 tumors per dose level using a varying intrinsic radiosensitivity described by the parameter σ_α in Table 1 [63, 64]. The dose level increment was realized by increasing the number of fractions rather than the fractional dose. The DPBN dose distributions were calculated by running the TRM with the mean radiosensitivity alpha parameter. An individual tumor was considered as controlled if no tumor cell survived. For each dose level, control rates were calculated as the ratio of controlled to total number of irradiated tumors. TCP curves were fitted to the control rates using a univariate logistic regression model, based on the mean dose to the tumor for each patient. TCP curves

were characterized by tumor control dose, D50 (dose at 50% TCP), which can be derived as the ratio of the two fitting coefficients of the logistic model [65]. Regarding the statistical analysis, a bootstrapping method was used to estimate the uncertainty associated to the D50 calculations [66]. Uncertainties are expressed with two standard deviations (coverage factor, k = 2). For each tumor type and DPBN adaptive scheme, treatment gain was calculated as the difference of D50 between the conventional uniform dose and the DPBN treatment (this is, *gain* = $D50_{conv} - D50_{DPBN}$).

Results

Tumors response to uniform dose distributions

The simulation of the response to conventional treatments with uniform dose distributions leads only to slightly different responses for the different tumors (see Fig 3A). As all tumors have the same number of tumor cells, a difference is only seen between the well oxygenated tumors (T2, T4) and the tumors with a hypoxic core (T1, T3). In accordance with this, the well oxygenated tumors (T2 and T4) have the same D50 values, which are lower than the D50 values of the hypoxic tumors, see Fig 3B. Focusing in the hypoxic tumors (T1 and T3), the slightly better outcome observed for T1 with respect to T3 is due to the observed higher degree of reoxygenation occurring in this tumor during the treatment. These TCP curves are in accordance with those observed from preclinical studies involving H&N xenografts from an intermediate radiosensitivity cell line (FaDu) and with a volume similar to the virtual tumors considered in our work [67]. The radiosensitivity α and β parameter values used in our simulations were taken from the literature [61, 62] and not specifically modified to fit to this experimental curve.

To illustrate the evolution of oxygenation during the course of the treatments, the status of the tumor core vf during the treatment is shown in Fig 4. The higher reoxygenation capability observed for the tumors with non-uniform tumor cell density (T1 and T4 reoxygenating more than T3 and T2, respectively) is due to the larger number of tumor cells killed in regions with high tumor cell density, which leads to a more pronounced tumor shrinkage associated with a stronger reoxygenation. This relationship has not been clinically proven and might not represent the true response of clinical tumors. However, as the reoxygenation-related

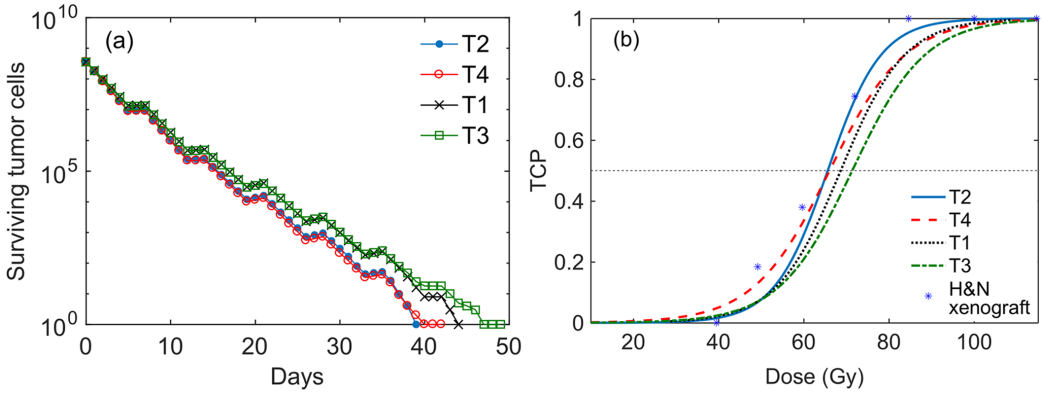

Fig 3. Tumor response to a uniform dose distribution. (a) Number of surviving tumor cells with time for the 4 tumor types irradiated with a uniform dose distribution. The weekend treatment breaks lead to small plateaus in the cells survival curves, in which the number of tumor cells increases slightly due to proliferation. (b) TCP curves for the simulated tumors and experimental response of a 200 mm^3 xenograft of the H&N FaDu line [67]. The $D50_{conv}$ values (in Gy) of the simulated TCP curves are 68.6 ± 1.4, 65.6 ± 2.1, 71.3 ± 2.0 and 66.0 ± 2.0, for T1, T2, T3 and T4 respectively.

https://doi.org/10.1371/journal.pone.0196310.g003

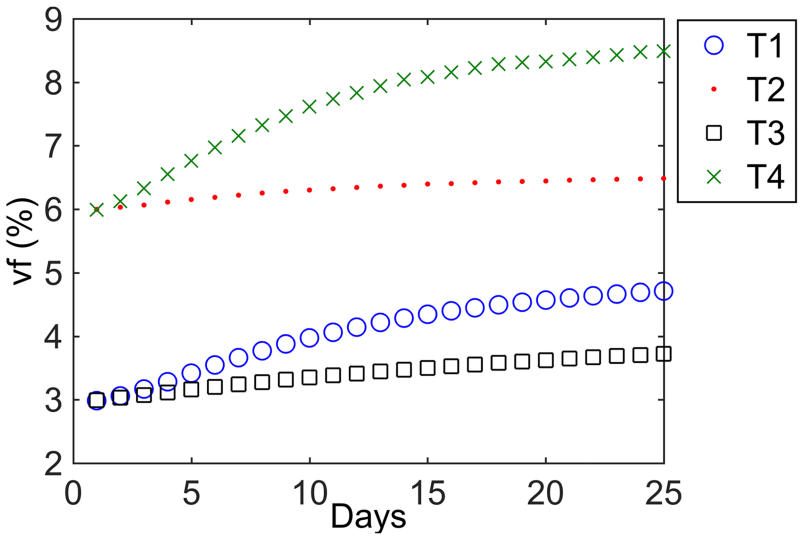

Fig 4. Radiation induced reoxygenation in the investigated virtual tumors. Evolution of the vascular fraction (averaged in the 1 cm diameter tumor core) for the 4 tumors when irradiated with a uniform dose distribution.

https://doi.org/10.1371/journal.pone.0196310.g004

radiosensitization might affect the treatment gain associated to DPBN, the use of virtual tumors with these distinct characteristics is considered of interest for the purpose of this work.

Tumors response to DPBN treatments

The response of the tumors to the DPBN treatments is presented in Fig 5 in terms treatment gain (T1 and T4, of higher reoxygenation capability, and T2 and T3, of lower reoxygenation capability). It is noted that DPBN applied to T1 and T4 exhibits significantly larger treatment

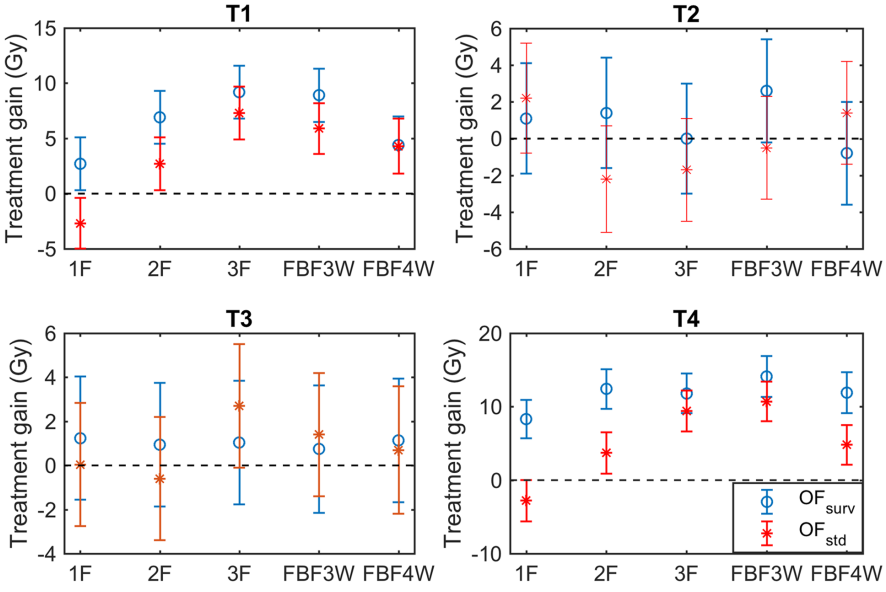

Fig 5. Treatment gains. Treatment gains obtained for the studied tumors (T1-T4) using dose distributions optimized with either OF_{surv} (○) or OF_{std} (*) under different adaptive schemes.

https://doi.org/10.1371/journal.pone.0196310.g005

gains, than for T2 and T3, where treatment gains are comparable with zero within uncertainties. Detailed D50 values leading to these treatment gains can be found in S1 Table.

Effect of the optimization objective function. Fig 5 shows that treatment gains are systematically larger for the DPBN treatments using OF_{surv} (minimization of survival) than for OF_{std} (minimization of heterogeneity). This is true under all the adaptive schemes investigated for tumors T1 and T4. Although treatment gains of T2 and T3 are not significant, they also exhibit systematically higher values with OF_{surv} in most of the cases.

Effect of different adaptive schemes. The responses observed under the different adaptive schemes depend again on the tumor type. For T2 and T3, outcomes for the conventional and the DPBN treatments are very similar (treatment gains comparable with zero within uncertainties, see Fig 5). Further analysis revealed that this observation is a result of the degree of vf heterogeneity and not due to the limited variation of dose allowed in this study (25% of 2 Gy). On the other hand, the DPBN treatments delivered to T1 and T4 exhibit treatment gains which generally increased with the number of dose distribution optimizations performed during the treatment ($gain_{1F} < gain_{2F} < gain_{3F} < gain_{FBF3W}$). However, only small differences between 3F and FBF3W were observed, and treatment gains for FBF4W decreased again relative to FBF3W. This is observed for both objective functions and was found to be related to the following reasons: i) As the DPBN treatment was optimized assuming a population-averaged radiosensitivity, the resulting dose distribution is slightly suboptimal for the individual tumors used to estimate TCP, ii) Another factor contributing to this is the small differences arising from the stochasticity of the cell killing, which becomes important towards the end of the treatment (when the number of tumor cells is small). For this reason, dose distributions were only optimized up to 4 weeks after the start of treatment. This effect also contributes to the finding that the treatment gains for FBF4W are not signicantly larger than for FBF3W.

To illustrate this effect, Fig 6 shows the response curves of T1 when irradiated with the FBF4W adaptive scheme using OF_{surv} under different assumptions. (i) When the dose distributions are optimized using one single tumor having the population-averaged radiosensitivity α, the tumor is controlled with 50 Gy. (ii) If the same treatment is delivered repeated times to this tumor to build a TCP curve, the cell killing stochasticity makes the response curve to become slightly shallow and D50 is (57.7 ± 1.0) Gy. (iii) If the radiosensitivity is additionally assumed to be normally distributed within a tumor population, D50 increases further to (64.2 ± 2.2) Gy and the slope is even more shallow.

Effect of tumor inhomogeneities. As shown above, the treatment gains achieved with the DPBN treatments were different for the 4 tumors, with values comparable with zero in some cases (T2 and T3). When the results for the 4 tumors are compared, a relationship between tumor reoxygenation capability and treatment gain can be observed: the higher the reoxygenation capability, the higher the treatment gain obtained from the DPBN treatment. Fig 7 shows the treatment gains associated to the DPBN treatments for both OFs and for the adaptive schemes leading to the higher treatment gains (3F, FBF3W and FBF4W). The tumors are ranked on the x-axis according to their reoxygenation capability ($reox_{T2} < reox_{T3} < reox_{T1} < reox_{T4}$).

Discussion

Comparison with other studies and limitations of this work

The present work studies DPBN by using a in-silico tumor response model that simultaneously considers several biological processes in the tumor during treatment. These processes are: oxygen-dependent cell survival after irradiation, proliferation of tumor cells, hypoxia-

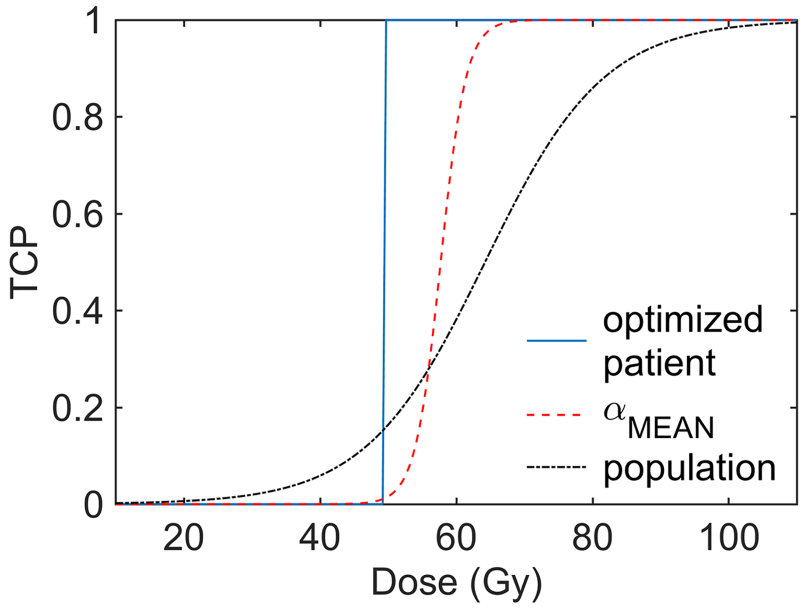

Fig 6. Sthocastic and population radiosensitivity variability effects. Response curves for tumor T1 when irradiated with the FBF4W scheme using OF_{surv}. Solid line, treatment response achieved when the treatment is optimized using the population-averaged radiosensitivity α; dashed line, TCP curve calculated using the same population-averaged radiosensitivity (the cell killing stochasticity produces the shallowing and displacement towards higher dose of the response curve); and dashed-dotted line, TCP curve calculated for a population with a normally distributed α radiosensitivity parameter (further shallowing and displacement).

https://doi.org/10.1371/journal.pone.0196310.g006

induced angiogenesis, resorption of dead cells, and tumor growth or shrinkage. These effects show complex interaction with tumor reoxygenation [46]. To our knowledge, no other study on the modelling of dose painting treatments considered these interacting biological processes altogether. Previous works either did not consider reoxygenation [13, 20, 22, 34], or simulated

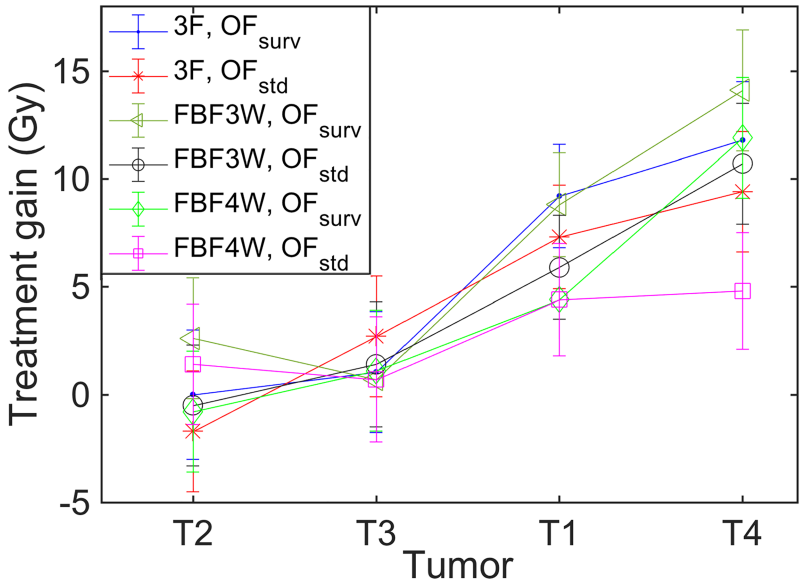

Fig 7. Impact of the adaptive scheme on treatment gain. Treatment gains associated to the DPBN treatments under the adaptive schemes 3F, FBF3W and FBF4W. Tumors ordered on the x-axis by ascending reoxygenation capability.

https://doi.org/10.1371/journal.pone.0196310.g007

it in a simplified way [23, 24, 47]. For example, some of them neglected tumor proliferation during treatment [24, 47] or decoupled it from reoxygenation [23], although both processes are known to be linked [68].

In this work we show that the dynamics of the biological processes during irradiation strongly affect the treatment results. Thus, to accurately model the radiation response of clinical tumors treated with radiotherapy using dose painting, three main aspects must be considered: i) a proper representation of the tumor oxygenation at a subvoxel scale [24, 49], ii) the spatial distribution of tumor cells [9, 20], and iii) realistic values of the biological parameters. In addition to the above mentioned aspects, we showed that the choice of the OF used for the DPBN optimization is also important. Minimizing the survival [9, 20, 24] was observed to lead to better treatment outcomes than minimizing the spatial heterogeneity of the surviving tumor cells, which had been investigated by [23, 37, 47]. The reason for this is that dose distributions calculated using OF_{std} change more drastically from fraction to fraction than those calculated using OF_{surv} (data not shown). Thus, when the tumor characteristics are measured only once or twice during treatment, the solution from OF_{surv} is closer to the optimal distribution that would have been calculated for the intermediate fractions. In this situation (only one or two optimizations), the use of OF_{std} would lead to lower local tumor control rates than the use of a uniform dose distribution. Consequently, the use of OF_{surv} would present a better choice for DPBN treatments.

In the study of different adaptive schemes, better treatment outcomes are observed when optimizations are performed at several time points of the treatment schedule, which is in agreement with the work of Sovik *et al.* 2007 [23]. The difference between fraction by fraction optimization schemes and optimizing 3 times (at the beginning of weeks 1, 3 and 4), was however found to be small. This is of great clinical advantage as a 3F scenario would be much implementable in the clinic, while performing daily measurements of the tumor characteristics with subsequent optimization is unfeasible. Other factors discouraging the use of fraction by fraction adapted dose distributions would be: i) uncertainties associated the measurement of tumor characteristics with molecular imaging (with radiation induced signal due to inflammation affecting some tenchiques like FDG) ii) lack of knowledge of individual tumor radiosensitivities, and iii) cell killing stochasticity, which may affect treatment response (being not reasonable to perform DPBN) in the late phase of the treatment.

Unfortunately, comparison of our results with experimental data is currently not possible. Several clinical trials have already implemented similar promising (2F or 3F) dose redistribution adaptive schemes, but for some of them, like the ARTFORCE trial [39], outcome data is still incomplete. Some other trials aimed at reducing normal tissue toxicity and thus results from these works are not comparable with ours [28, 45]. Amongst the few publications quantifying dose painting related treatment gain, the work recently published by Kong *et al.* shows that one (mid-treatment) FDG-PET based adaptation can result in locoregional tumor control improvement for patients with locally advanced Non-Small-Cell Lung Cancer [40]. However, this trial involved dose escalation and comparison of results with our dose redistribution approach is neither possible. One preclinical study [69] has investigated the use of dose redistribution with larger heterogeneities than the 25% allowed in our work. Trani *et al.* applied DPBC using 40% and 60% dose heterogeneity constraints, based on a pretreatment FDG-PET image, for single fraction irradiation of rhabdomyosarcomas [69]. Such dose redistributions were observed to be detrimental for tumor control with respect to the use of homogeneous dose distributions. This work did not involved the use of any radiobiology based dose distribution optimization though. Other trials have been focused on dose escalation, frequently aiming at endpoints different to tumor control [25, 41, 43, 44, 70].

This work was developed for the DPBN technique because it allows a more general voxel-based heterogeneity analysis. Results for the DPBC technique, also appropriate for tumors with relatively large subvolumes of uniform characteristics [71], should not be significantly different. Treatment gain values may change, but the authors would expect that DPBC plans using several (few) dose distribution optimizations should still be more beneficial for tumors with a higher reoxygenation capability than for poorly reoxygenating tumors. The effect of the optimization objective functions should also be the same for DPBN and DPBC.

We should notice that, in spite of the variety of interplaying dynamic biological processes considered in our work, the biological mechanisms arising in tumors during radiotherapy are very complex and not yet well understood, and our model makes simplifications about tumor growth and response. For example, only one type of tumor cells is considered, but it is well known that tumor cells with different degrees of differentiation conform the tumor, and that the initially small subpopulation of tumor stem cells plays an important role both in response and tumor repopulation [72]. We simulate, however, an average tumor cell radiosensitivity and proliferation parameter values based on experimental doubling times. Moreover, accelerated repopulation was modelled by using a single kick-off and doubling time, but there is evidence that such parameters may depend on tumor stage, number of viable tumor stem cells or hypoxia status [57, 73]. Tumor shrinkage in our model is due to undirected cell exchange, which may be also an oversimplification of the underlying process [74]. Cell death kinetics can affect the reoxygenation rate of tumors, but this effect is not relevant for conventional fractionation and vf above 3% [75].

A relevant aspect in DPBN is the choice of optimization constraints. The results presented here were derived from optimizations subjected to two constraints: i) a constant average dose constraint (2 Gy/fraction) and ii) a dose heterogeneity constraint of ±25% of 2 Gy, allowing doses from 1.5 to 2.5 Gy in each tumor voxel. No limits were however established for the allowed dose differences between neighboring voxels. Modern radiotherapy techniques are able to deliver strongly modulated dose distributions, however, the spatial resolution in the order of 5 mm may still be somewhat below that of the voxel size used in the TRM. Therefore, the use of smoother dose distributions might be clinically more feasible. Despite these discussed limitations, the trends observed in this work should not be qualitatively different from those observed in a clinical scenario.

Conclusion

Our study of DPBN with a computer-based tumor response model allowed us to gain insight into some factors affecting the treatment gain, like the optimization objective function, the tumor reoxygenation capability and the implemented adaptive scheme. Our study shows that tumors with high reoxygenation capability benefit more from DPBN. Additionally, the treatment gains of DPBN treatments in which dose distributions are optimized once a week are similar to those achieved with daily optimization. This indicates that only a few weekly optimizations, which is clinically more feasible, may be sufficient to improve the response of hypoxic tumors. This work shows that the dynamics of the biological processes arising in tumors during treatment have a relevant effect on dose distribution optimization. This evidences the need of not only a proper understanding of these processes but also quantitative information from functional imaging or any other methods.

Regarding the objective function, dose distributions optimized minimizing survival lead to better treatment outcomes than those optimized minimizing the spatial heterogeneity of the tumor cell survival.

Supporting information

S1 Table. Treatment outcomes data. Treatment outcomes for the investigated tumors quantified in terms of D50 values and treatment gains of DPBN treatments relative to irradiation with uniform dose. All values are expressed in Gy. DPBN treatments were optimized either with OF_{surv} or OF_{std}.
(PDF)

Acknowledgments

The authors thank the help of Andrés Pérez for the initial valuable discussions, especially concerning the use of the NEOS optimization server.

Author Contributions

Conceptualization: Araceli Gago-Arias, Beatriz Sánchez-Nieto, Ignacio Espinoza, Christian P. Karger, Juan Pardo-Montero.

Data curation: Araceli Gago-Arias.

Formal analysis: Araceli Gago-Arias, Beatriz Sánchez-Nieto, Ignacio Espinoza, Christian P. Karger, Juan Pardo-Montero.

Funding acquisition: Araceli Gago-Arias, Beatriz Sánchez-Nieto.

Investigation: Araceli Gago-Arias, Beatriz Sánchez-Nieto, Ignacio Espinoza, Christian P. Karger, Juan Pardo-Montero.

Methodology: Araceli Gago-Arias, Beatriz Sánchez-Nieto, Ignacio Espinoza, Christian P. Karger, Juan Pardo-Montero.

Project administration: Araceli Gago-Arias.

Resources: Araceli Gago-Arias.

Software: Araceli Gago-Arias, Ignacio Espinoza, Christian P. Karger.

Supervision: Araceli Gago-Arias, Beatriz Sánchez-Nieto, Juan Pardo-Montero.

Validation: Araceli Gago-Arias.

Visualization: Araceli Gago-Arias.

Writing – original draft: Araceli Gago-Arias.

Writing – review & editing: Araceli Gago-Arias, Beatriz Sánchez-Nieto, Ignacio Espinoza, Christian P. Karger, Juan Pardo-Montero.

References

1. Bentzen SM, Gregoire V; Elsevier. Molecular imaging–based dose painting: A novel paradigm for radiation therapy prescription. Semin Radiat Oncol. 2011; 21(2):101–110. https://doi.org/10.1016/j.semradonc.2010.10.001 PMID: 21356478
2. Gatenby RA, Kessler HB, Rosenblum JS, Coia LR, Moldofsky PJ, Hartz WH, et al. Oxygen distribution in squamous cell carcinoma metastases and its relationship to outcome of radiation therapy. Int J Radiat Oncol Biol Phys. 1988; 14(5):831–838. https://doi.org/10.1016/0360-3016(88)90002-8 PMID: 3360652
3. Höckel M, Knoop C, Schlenger K, Vorndran B, Baußnann E, Mitze M, et al. Intratumoral pO2 predicts survival in advanced cancer of the uterine cervix. Radiother Oncol. 1993; 26(1):45–50. https://doi.org/10.1016/0167-8140(93)90025-4 PMID: 8438086

4. Movsas B, Chapman JD, Hanlon AL, Horwitz EM, Greenberg RE, Stobbe C, et al. Hypoxic prostate/muscle pO 2 ratio predicts for biochemical failure in patients with prostate cancer: preliminary findings. Urology. 2002; 60(4):634–639. https://doi.org/10.1016/S0090-4295(02)01858-7 PMID: 12385924
5. Zelefsky MJ, Levin EJ, Hunt M, Yamada Y, Shippy AM, Jackson A, et al. Incidence of late rectal and urinary toxicities after three-dimensional conformal radiotherapy and intensity-modulated radiotherapy for localized prostate cancer. Int J Radiat Oncol Biol Phys. 2008; 70(4):1124–1129. https://doi.org/10.1016/j.ijrobp.2007.11.044 PMID: 18313526
6. Cox JD. Are the results of RTOG 0617 mysterious? Int J Radiat Oncol Biol Phys. 2012; 82(3):1042–1044. https://doi.org/10.1016/j.ijrobp.2011.12.032 PMID: 22284026
7. Brahme A, Argren A. Optimal dose distribution for eradication of heterogeneous tumors. Acta Oncol. 1987; 26(5):377–385. https://doi.org/10.3109/02841868709104364 PMID: 3426851
8. Zagars GK, Schultheiss TE, Peters LJ. Inter-tumor heterogeneity and radiation dose-control curves. Radiother Oncol. 1987; 8(4):353–361. https://doi.org/10.1016/S0167-8140(87)80186-X PMID: 3588999
9. Ebert M, Hoban P. Some characteristics of tumour control probability for heterogeneous tumours. Phys Med Biol. 1996; 41(10):2125. https://doi.org/10.1088/0031-9155/41/10/019 PMID: 8912385
10. Zhang Q, Tian S, Borasi G. A new definition of biological effective dose: The dose distribution effects. Phys Med. 2015; 31(8):1060–1064. https://doi.org/10.1016/j.ejmp.2015.07.145 PMID: 26429382
11. Sánchez-Nieto B, Nahum AE. The delta-TCP concept: a clinically useful measure of tumor control probability. Int J Radiat Oncol Biol Phys. 44(2):369–380. https://doi.org/10.1016/S0360-3016(99)00029-2 PMID: 10760433
12. Ling CC, Humm J, Larson S, Amols H, Fuks Z, Leibel S, et al. Towards multidimensional radiotherapy (MD-CRT): biological imaging and biological conformality. Int J Radiat Oncol Biol Phys. 2000; 47(3):551–560. https://doi.org/10.1016/S0360-3016(00)00467-3 PMID: 10837935
13. Das SK, Ten Haken RK; Elsevier. Functional and molecular image guidance in radiotherapy treatment planning optimization. Semin Radiat Oncol. 2011; 21(2):111–118. https://doi.org/10.1016/j.semradonc.2010.10.002 PMID: 21356479
14. Jeraj R, Bradshaw T, Simončič U. Molecular imaging to plan radiotherapy and evaluate its efficacy. J Nucl Med. 2015; 56(11):1752–1765. https://doi.org/10.2967/jnumed.114.141424 PMID: 26383148
15. Shi X, Meng X, Sun X, Xing L, Yu J. PET/CT imaging-guided dose painting in radiation therapy. Cancer letters. 2014; 355(2):169–175. https://doi.org/10.1016/j.canlet.2014.07.042 PMID: 25218590
16. Chao KC, Bosch WR, Mutic S, Lewis JS, Dehdashti F, Mintun MA, et al. A novel approach to overcome hypoxic tumor resistance: Cu-ATSM-guided intensity-modulated radiation therapy. Int J Radiat Oncol Biol Phys. 2001; 49(4):1171–1182. https://doi.org/10.1016/S0360-3016(00)01433-4 PMID: 11240261
17. Nutting C, Corbishley C, Sánchez-Nieto B, Cosgrove V, Webb S, Dearnaley D. Potential improvements in the therapeutic ratio of prostate cancer irradiation: dose escalation of pathologically identified tumour nodules using intensity modulated radiotherapy. Br J Radiol. 2002; 75(890):151–161. https://doi.org/10.1259/bjr.75.890.750151 PMID: 11893639
18. Alber M, Paulsen F, Eschmann S, Machulla H. On biologically conformal boost dose optimization. Phys Med Biol. 2003; 48(2):N31–N35. https://doi.org/10.1088/0031-9155/48/2/404 PMID: 12587912
19. Bentzen SM. Theragnostic imaging for radiation oncology: dose-painting by numbers. Lancet Oncol. 2005; 6(2):112–117. https://doi.org/10.1016/S1470-2045(05)01737-7 PMID: 15683820
20. Yang Y, Xing L. Towards biologically conformal radiation therapy (BCRT): selective IMRT dose escalation under the guidance of spatial biology distribution. Med Phys. 2005; 32(6):1473–1484. https://doi.org/10.1118/1.1924312 PMID: 16013703
21. Vanderstraeten B, Duthoy W, De Gersem W, De Neve W, Thierens H. [18 F] fluoro-deoxy-glucose positron emission tomography ([18 F] FDG-PET) voxel intensity-based intensity-modulated radiation therapy (IMRT) for head and neck cancer. Radiother Oncol. 2006; 79(3):249–258. https://doi.org/10.1016/j.radonc.2006.03.003 PMID: 16564588
22. Flynn R, Barbee D, Bowen S, McCall K, Bentzen S, Mackie T, et al. MO-D-M100J-01: Dose Painting With Intensity Modulated Proton Therapy and Intensity Modulated X-Ray Therapy: A Comparison. Med Phys. 2007; 34(6):2522–2523. https://doi.org/10.1118/1.2761242
23. Søvik Å, Malinen E, Bruland ØS, Bentzen SM, Olsen DR. Optimization of tumour control probability in hypoxic tumours by radiation dose redistribution: a modelling study. Phys Med Biol. 2006; 52(2):499. PMID: 17202629
24. Petit SF, Dekker AL, Seigneuric R, Murrer L, van Riel NA, Nordsmark M, et al. Intra-voxel heterogeneity influences the dose prescription for dose-painting with radiotherapy: a modelling study. Phys Med Biol. 2009; 54(7):2179. https://doi.org/10.1088/0031-9155/54/7/022 PMID: 19293465

25. Madani I, Duthoy W, Derie C, De Gersem W, Boterberg T, Saerens M, et al. Positron emission tomography-guided, focal-dose escalation using intensity-modulated radiotherapy for head and neck cancer. Int J Radiat Oncol Biol Phys. 2007; 68(1):126–135. https://doi.org/10.1016/j.ijrobp.2006.12.070 PMID: 17448871

26. Duprez F, De Neve W, De Gersem W, Coghe M, Madani I. Adaptive dose painting by numbers for head-and-neck cancer. Int J Radiat Oncol Biol Phys. 2011; 80(4):1045–1055. https://doi.org/10.1016/j.ijrobp.2010.03.028 PMID: 20643512

27. Kong F, Ten Haken RK, Schipper MJ, Hayman J, Ramnath N, Hassan KA, et al. A phase II trial of mid-treatment FDG-PET adaptive, individualized radiation therapy plus concurrent chemotherapy in patients with non-small cell lung cancer (NSCLC). J Clin Oncol. 2013; 31 Suppl 15:7522.

28. Berwouts D, Olteanu LA, Duprez F, Vercauteren T, De Gersem W, De Neve W, et al. Three-phase adaptive dose-painting-by-numbers for head-and-neck cancer: initial results of the phase I clinical trial. Radiother Oncol. 2013; 107(3):310–316. https://doi.org/10.1016/j.radonc.2013.04.002 PMID: 23647760

29. Grönlund E, Johansson S, Montelius A, Ahnesjö A. Dose painting by numbers based on retrospectively determined recurrence probabilities. Radiother Oncol. 2017; 122(2):236–241. https://doi.org/10.1016/j.radonc.2016.09.007 PMID: 27707505

30. Lee NY, Mechalakos JG, Nehmeh S, Lin Z, Squire OD, Cai S, et al. Fluorine-18-labeled fluoromisonidazole positron emission and computed tomography-guided intensity-modulated radiotherapy for head and neck cancer: a feasibility study. Int J Radiat Oncol Biol Phys. 2008; 70(1):2–13. https://doi.org/10.1016/j.ijrobp.2007.06.039 PMID: 17869020

31. Choi W, Lee Sw, Park SH, Ryu JS, Oh SJ, Im KC, et al. Planning study for available dose of hypoxic tumor volume using fluorine-18-labeled fluoromisonidazole positron emission tomography for treatment of the head and neck cancer. Radiother Oncol. 2010; 97(2):176–182. https://doi.org/10.1016/j.radonc.2010.04.012 PMID: 20855118

32. Chang JH, Wada M, Anderson NJ, Lim Joon D, Lee ST, Gong SJ, et al. Hypoxia-targeted radiotherapy dose painting for head and neck cancer using 18F-FMISO PET: a biological modeling study. Acta Oncol. 2013; 52(8):1723–1729. https://doi.org/10.3109/0284186X.2012.759273 PMID: 23317145

33. Troost EG, Bussink J, Hoffmann AL, Boerman OC, Oyen WJ, Kaanders JH. 18F-FLT PET/CT for early response monitoring and dose escalation in oropharyngeal tumors. J Nucl Med. 2010; 51(6):866–874. https://doi.org/10.2967/jnumed.109.069310 PMID: 20484426

34. Dirscherl T, Rickhey M, Bogner L. Feasibility of TCP-based dose painting by numbers applied to a prostate case with 18 F-choline PET imaging. Z Med Phys. 2012; 22(1):48–57. https://doi.org/10.1016/j.zemedi.2011.09.006 PMID: 22047806

35. Das S, Miften M, Zhou S, Bell M, Munley M, Whiddon C, et al. Feasibility of optimizing the dose distribution in lung tumors using fluorine-18-fluorodeoxyglucose positron emission tomography and single photon emission computed tomography guided dose prescriptions. Med Phys. 2004; 31(6):1452–1461. https://doi.org/10.1118/1.1750991 PMID: 15259648

36. Thorwarth D, Eschmann SM, Paulsen F, Alber M. A kinetic model for dynamic [18F]-Fmiso PET data to analyse tumour hypoxia. Phys Med Biol. 2005; 50(10):2209. https://doi.org/10.1088/0031-9155/50/10/002 PMID: 15876662

37. Thorwarth D, Eschmann SM, Paulsen F, Alber M. Hypoxia dose painting by numbers: a planning study. Int J Radiat Oncol Biol Phys. 2007; 68(1):291–300. https://doi.org/10.1016/j.ijrobp.2006.11.061 PMID: 17448882

38. Bowen SR, Flynn RT, Bentzen SM, Jeraj R. On the sensitivity of IMRT dose optimization to the mathematical form of a biological imaging-based prescription function. Phys Med Biol. 2009; 54(6):1483. https://doi.org/10.1088/0031-9155/54/6/007 PMID: 19218733

39. Heukelom J, Hamming O, Bartelink H, Hoebers F, Giralt J, Herlestam T, et al. Adaptive and innovative Radiation Treatment FOR improving Cancer treatment outcomE (ARTFORCE); a randomized controlled phase II trial for individualized treatment of head and neck cancer. BMC cancer. 2013; 13(1):84. https://doi.org/10.1186/1471-2407-13-84 PMID: 23433435

40. Kong FM, Ten Haken RK, Schipper M, Frey KA, Hayman J, Gross M, et al. Effect of Midtreatment PET/CT-Adapted Radiation Therapy With Concurrent Chemotherapy in Patients With Locally Advanced Non–Small-Cell Lung Cancer: A Phase 2 Clinical Trial. JAMA oncology. 2017;. https://doi.org/10.1001/jamaoncol.2017.0982 PMID: 28570742

41. Madani I, Duprez F, Boterberg T, Van de Wiele C, Bonte K, Deron P, et al. Maximum tolerated dose in a phase I trial on adaptive dose painting by numbers for head and neck cancer. Radiother Oncol. 2011; 101(3):351–355. https://doi.org/10.1016/j.radonc.2011.06.020 PMID: 21742392

42. Berwouts D, Olteanu LAM, Speleers B, Duprez F, Madani I, Vercauteren T, et al. Intensity modulated arc therapy implementation in a three phase adaptive 18 F-FDG-PET voxel intensity-based planning

strategy for head-and-neck cancer. Radiat Oncol. 2016; 11(1):52. https://doi.org/10.1186/s13014-016-0629-3 PMID: 27039294

43. Kachnic LA, Winter K, Myerson RJ, Goodyear MD, Willins J, Esthappan J, et al. RTOG 0529: a phase 2 evaluation of dose-painted intensity modulated radiation therapy in combination with 5-fluorouracil and mitomycin-C for the reduction of acute morbidity in carcinoma of the anal canal. Int J Radiat Oncol Biol Phys. 2013; 86(1):27–33. https://doi.org/10.1016/j.ijrobp.2012.09.023 PMID: 23154075

44. Onjukka E, Uzan J, Baker C, Howard L, Nahum A, Syndikus I. Twenty Fraction Prostate Radiotherapy with Intra-prostatic Boost: Results of a Pilot Study. Clin Oncol. 2017; 29(1):6–14. https://doi.org/10.1016/j.clon.2016.09.009

45. Berwouts D, De Wolf K, Lambert B, Bultijnck R, De Neve W, De Lobel L, et al. Biological 18 [F]-FDG-PET image-guided dose painting by numbers for painful uncomplicated bone metastases: A 3-arm randomized phase II trial. Radiother Oncol. 2015; 115(2):272–278. https://doi.org/10.1016/j.radonc.2015.04.022 PMID: 25981049

46. Espinoza I, Peschke P, Karger C. A voxel-based multiscale model to simulate the radiation response of hypoxic tumors. Med Phys. 2015; 42(1):90–102. https://doi.org/10.1118/1.4903298 PMID: 25563250

47. Toma-Daşu I, Daşu A, Brahme A. Dose prescription and optimisation based on tumour hypoxia. Acta Oncol. 2009; 48(8):1181–1192. https://doi.org/10.3109/02841860903188643 PMID: 19863227

48. Fowler JF. The linear-quadratic formula and progress in fractionated radiotherapy. Br J Radiol. 1989; 62(740):679–694. https://doi.org/10.1259/0007-1285-62-740-679 PMID: 2670032

49. Wouters BG, Brown JM. Cells at intermediate oxygen levels can be more important than the "hypoxic fraction" in determining tumor response to fractionated radiotherapy. Radiat Res. 1997; 147(5):541–550. https://doi.org/10.2307/3579620 PMID: 9146699

50. Espinoza I, Peschke P, Karger CP. A model to simulate the oxygen distribution in hypoxic tumors for different vascular architectures. Med Phys. 2013; 40(8). https://doi.org/10.1118/1.4812431

51. Gropp W, Moré J. Optimization environments and the NEOS server. In: Buhmann M. D. and Iserles A., editors. Approximation theory and optimization, Cambridge University Press Cambridge, UK. 1997; p. 167–182.

52. Czyzyk J, Mesnier MP, Moré JJ. The NEOS server. IEEE Comput Sci Eng. 1998; 5(3):68–75. https://doi.org/10.1109/99.714603

53. Steel G. Basic clinical radiobiology. Arnold, London. Oxford University Press; 2002.

54. Bremer C, Mustafa M, Bogdanov A Jr, Ntziachristos V, Petrovsky A, Weissleder R. Steady-state blood volume measurements in experimental tumors with different angiogenic burdens?a study in mice. Radiology. 2003; 226(1):214–220. https://doi.org/10.1148/radiol.2261012140 PMID: 12511693

55. Mönnich D, Troost EG, Kaanders JH, Oyen WJ, Alber M, Thorwarth D. Modelling and simulation of [18F] fluoromisonidazole dynamics based on histology-derived microvessel maps. Phys Med Biol. 2011; 56(7):2045. https://doi.org/10.1088/0031-9155/56/7/009 PMID: 21386142

56. Withers H, Taylor J, Maciejewski B. The hazard of accelerated tumor clonogen repopulation during radiotherapy. Acta Oncol. 1988; 27(2):131–146. https://doi.org/10.3109/02841868809090333 PMID: 3390344

57. Harriss-Phillips WM, Bezak E, Yeoh E. The HYP-RT hypoxic tumour radiotherapy algorithm and accelerated repopulation dose per fraction study. Study Comput Math Methods Med. 2012; 2012. https://doi.org/10.1155/2012/363564 PMID: 22778783

58. Denekamp J, Hobson B. Endothelial-cell proliferation in experimental tumours. Br J Cancer. 1982; 46 (5):711. https://doi.org/10.1038/bjc.1982.263 PMID: 7171453

59. Denekamp J. Endothelial cell proliferation as a novel approach to targeting tumour therapy. Br J Cancer. 1982; 45(1):136. https://doi.org/10.1038/bjc.1982.16 PMID: 7059456

60. Harting C, Peschke P, Borkenstein K, Karger CP. Single-cell-based computer simulation of the oxygen-dependent tumour response to irradiation. Phys Med Biol. 2007; 52(16):4775. https://doi.org/10.1088/0031-9155/52/16/005 PMID: 17671335

61. Schwachöfer J, Crooijmans R, Van Gasteren J, Hoogenhout J, Jerusalem C, Kal H, et al. Radiosensitivity of different human tumor cell lines grown as multicellular spheroids determined from growth curves and survival data. Int J Radiat Oncol Biol Phys. 1989; 17(5):1015–1020. https://doi.org/10.1016/0360-3016(89)90149-1 PMID: 2808034

62. Fowler J. Optimum overall times II: Extended modelling for head and neck radiotherapy. Clin Oncol. 2008; 20(2):113–126. https://doi.org/10.1016/j.clon.2007.11.003

63. Nahum AE, Movsas B, Horwitz EM, Stobbe CC, Chapman JD. Incorporating clinical measurements of hypoxia into tumor local control modeling of prostate cancer: implications for the α/β ratio. Int J Radiat Oncol Biol Phys. 2003; 57(2):391–401. https://doi.org/10.1016/S0360-3016(03)00534-0 PMID: 12957250

64. Moiseenko V. Effect of heterogeneity in radiosensitivity on LQ based isoeffect formalism for low α/β cancers. Acta Oncol. 2004; 43(5):499–502. https://doi.org/10.1080/02841860410032777 PMID: 15360056

65. Banerjee H. Estimation of parameters for logistic regression model in dose response study with a single compound or mixture of compounds [dissertation]. University of California, Riverside; 2010.

66. El Naqa I, Bradley J, Blanco AI, Lindsay PE, Vicic M, Hope A, et al. Multivariable modeling of radiotherapy outcomes, including dose–volume and clinical factors. Int J Radiat Oncol Biol Phys. 2006; 64 (4):1275–1286. https://doi.org/10.1016/j.ijrobp.2005.11.022 PMID: 16504765

67. Yaromina A, Kroeber T, Meinzer A, Boeke S, Thames H, Baumann M, et al. Exploratory study of the prognostic value of microenvironmental parameters during fractionated irradiation in human squamous cell carcinoma xenografts. Int J Radiation Oncology Biol Phys. 2011; 80(4):1205–1213. https://doi.org/10.1016/j.ijrobp.2011.02.015

68. Zhang C, Cao S, Xu Y. Population dynamics inside cancer biomass driven by repeated hypoxia-reoxygenation cycles. Quant Biol. 2014; 2(3):85–99. https://doi.org/10.1007/s40484-014-0032-8

69. Trani D, Yaromina A, Dubois L, Granzier M, Peeters SG, Biemans R, et al. Preclinical assessment of efficacy of radiation dose painting based on intratumoral FDG-PET uptake. Clin Cancer Res. 2015; 21(24):5511–5518. https://doi.org/10.1158/1078-0432.CCR-15-0290 PMID: 26276892

70. Fleckenstein J, Hellwig D, Kremp S, Grgic A, Gröschel A, Kirsch CM, et al. F-18-FDG-PET confined radiotherapy of locally advanced NSCLC with concomitant chemotherapy: results of the PET-PLAN pilot trial. Int J Radiat Oncol Biol Phys. 2011; 81(4):e283–e289. https://doi.org/10.1016/j.ijrobp.2011.01.020 PMID: 21470782

71. Brahme A. Dosimetric precision requirements and quantities for characterizing the response of tumors and normal tissues. IAEA-TECDOC-896. 1996; p. 49–65.

72. Marcu L, Van Doorn T, Olver I. Modelling of post-irradiation accelerated repopulation in squamous cell carcinomas. Phys Med Biol. 2004; 49(16):3767. https://doi.org/10.1088/0031-9155/49/16/021 PMID: 15446804

73. Pedicini P, Strigari L, Benassi M. Estimation of a self-consistent set of radiobiological parameters from hypofractionated versus standard radiation therapy of prostate cancer. Int J Radiat Oncol Biol Phys. 2013; 85(5):e231–e237. https://doi.org/10.1016/j.ijrobp.2012.11.033 PMID: 23332226

74. Huang Z, Mayr NA, Yuh WT, Lo SS, Montebello JF, Grecula JC, et al. Predicting outcomes in cervical cancer: a kinetic model of tumor regression during radiation therapy. Cancer Res. 2010; 70(2):463–470. https://doi.org/10.1158/0008-5472.CAN-09-2501 PMID: 20068180

75. Gago-Arias A, Aguiar P, Espinoza I, Sánchez-Nieto B, Pardo-Montero J. Modelling radiation-induced cell death and tumour re-oxygenation: local versus global and instant versus delayed cell death. Phys Med Biol. 2016; 61(3):1204. https://doi.org/10.1088/0031-9155/61/3/1204 PMID: 26788751